Analysis of Intracellular Fatty Acid Metabolism in Senescent Cells using Raman Microscopy

Swarang Sachin Pundlik[1], *Ashwin Venkateshvaran*[1, 2], *Hitesh Mamgain*[3], *Arvind Ramanathan*[1, *]

1. Metabolic Regulation of Cell Fate (RCF), Institute for Stem Cell Science and Regenerative Medicine (BRIC-InStem), GKVK – Post, Bellary Road, Bengaluru – 560065.

2. Tata Institute for Genetics and Society, Gandhi Krishi Vignana Kendra, Rajiv Gandhi Nagar, Kodigehalli, Bengaluru, Karnataka – 560065.

3. Wissenschaftliche Instrumente und Technologie (WITec) GmbH, Oxford Instruments India Pvt. Ltd., Nehru Nagar, Wagle Industrial Estate, Thane (W) – 400604.

KEYWORDS: Raman Microscopy, Hyperspectral Imaging, Lipid Metabolism, Arachidonic Acid Metabolism.

Abstract

Cellular senescence is a permanent growth arrest triggered by stressors such as DNA damage, contributing both to tumor suppression and to age-associated dysfunction through the senescence-associated secretory phenotype (SASP). Lipid remodeling is a key but poorly understood feature of this state. Here, we apply hyperspectral Raman microscopy to visualize lipid accumulation and fatty acid metabolism in senescent human breast adenocarcinoma (MCF7) cells. Senescence was induced by Doxorubicin treatment and validated by morphology, p21 expression, and senescence-associated β-galactosidase activity. Raman imaging revealed progressive enrichment of CH_2 stretching signals at 2850 cm^{-1} across 10–25 days post-treatment. Principal component analysis (PCA) distinguished proliferating and senescent cells with variance explained largely by lipid vibrational modes, including CH_2 scissoring (1445 cm^{-1}), C=C stretching (1655 cm^{-1}), and CH_2 stretching (2850 cm^{-1}), indicating a marked compositional transition between 15 and 18 days of senescence. To probe functional lipid metabolism, we employed deuterated arachidonic acid (AA-d_8), which displays unique (C=C)-D stretching peaks at 2220 and 2254 cm^{-1} within the silent Raman region. In vitro assays confirmed that cyclooxygenase-2 (COX2) metabolism of AA-d_8 leads to a time-dependent reduction of these peaks relative to lipid signals. In senescent MCF7 cells, AA-d_8 accumulated perinuclearly and showed heterogeneous distribution. Withdrawal of the COX2 inhibitor Cay-10404 resulted in a progressive decrease of the (C=C)-D peaks normalized to total lipids, consistent with intracellular arachidonic acid metabolism. Together, these results establish hyperspectral Raman microscopy as a label-free platform to resolve senescence-associated lipid remodeling and metabolic heterogeneity. By enabling spatial and temporal detection of fatty acid metabolism,

this approach provides a powerful tool for dissecting senescence biology and supports future strategies to identify, monitor, and target senescent cells in disease and aging contexts.

Introduction

Senescent cells accumulate following cytotoxic stress and contribute to both tumor suppression and age-related pathologies. Treatment with DNA-damaging agents such as Doxorubicin (Doxo) has been shown to induce senescence in both malignant and non-malignant cells[1–3]. Once established, senescent cells develop a senescence-associated secretory phenotype (SASP) and release a wide spectrum of bioactive molecules, including lipids and lipid-derived metabolites, that alter neighboring cell physiology and disrupt tissue homeostasis[4–8]. Mapping the spatial and temporal dynamics of lipid remodeling during senescence is therefore critical for understanding disease mechanisms and for informing therapeutic strategies. Conventional approaches for probing intracellular lipid distribution are limited by extensive sample preparation and the need for chemical derivatization. In contrast, Raman effect–based microscopy enables the direct spatial detection of biomolecules in intact samples without labeling or specialized preparation. By exploiting inelastic scattering signatures, this method provides a label-free window into the intracellular distribution of lipids[9]. In this study, we applied hyperspectral Raman imaging to senescent MCF7 human breast adenocarcinoma cells at defined stages of DNA damage–mediated senescence, and used principal component analysis (PCA) to identify characteristic differences in Raman spectra across senescence progression.

Methods

Cell culture and Treatment:

MCF7 Human breast adenocarcinoma cells (HTB-22) were maintained in DMEM supplemented with 10% FBS and 1% Penicillin-Streptomycin (DMEM–10%FBS medium) @37°C, 5% CO_2. Cells were seeded in glass-bottom dishes for experiments. Doxorubicin dissolved in DMSO was diluted in DMEM – 10% FBS medium. MCF7 cells were treated with

Doxorubicin (150 nM) for 5 days. The cells were then incubated in DMEM – 10% FBS medium till the end of the experiments. Deuterated Arachidonic Acid (AA-d8) and Cay-10404 (Cayman Chemical Company) were dissolved in DMSO and diluted in DMEM – 10% FBS medium. MCF7 cells were treated with Cay-10404 (30 μM) in DMEM-10% FBS medium for 2 hours. Cells were then treated with AA-d8 (100 μM) and Cay-10404 (30 μM) in DMEM-10%FBS medium overnight.

Hyperspectral Raman Imaging:

MCF7 cells were fixed with 4% paraformaldehyde at room temperature for 5 minutes. The cells were then washed thrice with Dulbecco's Phosphate Buffer Saline (DPBS) and were kept in DPBS during Raman imaging. Hyperspectral Raman Imaging was done using a WITec alpha 300Ri microscope (WITec GmbH). Images were recorded on WITec control six (WITec) software using the following parameters: Objective: 40x, Pixel Size: 500 nm/pixel, Laser wavelength: 532 nm, Laser Power: 60 mW, Acquisition time: 2 seconds/Pixel, Spectral Grating: 600 mm^{-1}.

To measure the *in vitro* metabolism of Arachidonic Acid, AA-d8 (100 μM) was incubated with COX2 enzyme (Cayman Chemical Company) in the reaction buffer (Tris-Cl (100 mM) pH=8, EDTA (5 mM), Hematin (100 nM), Phenol (500 μM)). At the end of the reaction, the samples were flash-frozen in liq. N_2 and stored @-80°C. lipid extraction was done by the methanol-formic acid-ethyl acetate method[10]. The lipid extract was dried and resuspended in ethyl acetate. The samples were spotted on glass coverslips, and Raman spectra were recorded on the alpha 300 Ri microscope (WITec GmbH) using the following parameters: Objective: 40x, Laser Wavelength: 532 nm, Laser Power: 60 mW, Acquisition time: 25 seconds, Spectral Grating: 600 mm^{-1}.

Imaging Processing:

For PCA, hyperspectral Raman images were exported as MATLAB files from WITec Project Six (WITec) software. Batch processing of the MATLAB files was done by the RamanSPy package[11] using a custom Python script followed by PCA and projected loadings analysis (Appendix I).

For measuring Arachidonic Acid Metabolism, hyperspectral Raman images of MCF7 cells were processed in WITec Project Six software (WITec) for cosmic ray removal and background correction. Spectral heatmaps of the integrated areas for the (C=C)-D Stretching peaks (2220±17.5 cm^{-1} and 2254±17.5 cm^{-1}) and CH_2 Stretching peak (2850±15 cm^{-1}) were obtained. Ratiometric image analysis was done using ImageJ (NIH) to obtain normalized heatmaps of (C=C)-D stretching peaks to CH_2 stretching peak.

Results and Discussion

We induced senescence in MCF7 cells by treatment with Doxo (150 nM for 5 days), followed by culture in DMEM supplemented with 10% FBS. Senescence induction was confirmed through morphological changes, nuclear enlargement, p21 expression and localization, and senescence-associated β-galactosidase activity[12] (Figure S1A–C). Cells were fixed at days 10, 15, 18, and 25 post-treatment and analyzed by hyperspectral Raman imaging, with proliferating cells serving as controls. Pixel-resolved Raman spectra were acquired from both proliferating and senescent populations (Figure 1A). Lipid accumulation, assessed by the integrated area of the CH_2 stretching peak at 2850 cm^{-1}, increased progressively in Doxo-treated cells (Figure 1B), consistent with earlier observations[13]. Pre-processing of the hyperspectral Raman images (Denoising, Cosmic Ray Removal, Background Subtraction, Normalization) was performed in Python using the RamanSPy package[11]. PCA of the pre-processed Raman images revealed clear

segregation of proliferating versus senescent cells: proliferating and 15-day senescent cells differed by 66% variance, and proliferating versus 25-day senescent cells by 76% variance (Figure S1D). In contrast, spectra from proliferating cells overlapped with those of 10- and 15-day senescent cells (Figure S1E, F), whereas divergence became apparent by days 18 and 25 (Figure S1G; Figure 1C). These data suggest a major intracellular compositional shift occurring between 15 and 18 days of senescence. Spectral loadings demonstrated that lipid-related vibrational modes were principal contributors to separation: CH_2 scissoring at 1445 cm^{-1} accounted for ~12% of the variance, C=C stretching at 1655 cm^{-1} contributed ~3%, and CH_2 stretching at 2850 cm^{-1} contributed ~8–10%. These findings indicate that fatty acid–associated spectral shifts underlie the differentiation of proliferating and senescent cell states by hyperspectral Raman imaging. Together, the results establish that Raman microscopy, coupled with PCA, can resolve senescence-associated lipid remodeling with high specificity. This capability highlights the potential to identify senescent cell niches in tissues in a label-free manner, enabling strategies for selective targeting of senescent cells in aging and disease.

Senescent cells show increased accumulation of Polyunsaturated Fatty Acids (PUFA), including Arachidonic Acid[8]. Senescent cells also show increased metabolism of Arachidonic Acid leading to synthesis and release of several classes of oxylipins, including prostaglandins[8,10]. Therefore, we measured the metabolism of arachidonic acid in senescent cells using Raman microscopy. Arachidonic Acid (20:4) is a polyunsaturated fatty acid that shows characteristic spectral shifts at wave numbers 1655 cm^{-1} and 3005 cm^{-1} that correspond to C=C stretching and (C=C)-H stretching, respectively (Figure S2A). Arachidonic Acid with deuterium atoms across all the double bonds shows the presence of a characteristic spectral shift corresponding to (C=C)-D stretching at ~2240 cm^{-1} (Figure S2A, Figure 2A) in the biologically silent region[14].

Measuring the changes in the (C=C)-D stretching peaks is advantageous due to the high signal-to-noise ratio in the otherwise silent region, allowing measurement of chemical changes only in the labelled molecule. Therefore, we used deuterated Arachidonic Acid (AA-d8) to measure the intracellular metabolism of Arachidonic Acid in senescent cells. We observed that the Raman spectrum of AA-d8 shows two peaks corresponding to (C=C)-D stretching, one at 2220 cm^{-1} (minor peak) and another at 2254 cm^{-1} (major peak), suggesting two vibrational modes of (C=C)-D stretching (Figure 2A). We hypothesized that the metabolism of arachidonic acid can be measured by changes in the vibrational modes of the (C=C)-D bond, which can be monitored by changes in the Raman signatures. We tested the hypothesis by *in vitro* metabolism of AA-d8 by the COX2 enzyme (Figure S2B) and measuring the changes in the spectral shifts. We did not observe any change in the wavenumber of the spectral shifts in the (C=C)-D peaks (Figure S2C), suggesting no change in the vibrational modes of (C=C)-D stretching. We then measured any changes in the relative intensities of the (C=C)-D peaks (2220 cm^{-1} and 2254 cm^{-1}) to the CH_2 stretching peaks (2850 cm^{-1}) during COX2-mediated metabolism of arachidonic acid. We observed a time-dependent decrease in the intensities of the (C=C)-D peaks relative to the CH_2 Stretching peaks during COX2-mediated metabolism of AA-d8, suggesting that the relative intensities of the (C=C)-D peaks can be used to measure metabolism of Arachidonic Acid. So, to measure the metabolism of arachidonic acid in senescent cells, we treated ~15-day senescent MCF7 cells with AA-d8 (100 μM) overnight and observed complete cell death (data not shown). We hypothesized that the cell death observed after treating senescent cells with AA-d8 overnight is because of the cytotoxic effects of arachidonic acid metabolites, a phenotype we observed in a previous study[10]. Therefore, we pretreated senescent MCF7 cells with Cay-10404, an inhibitor of COX2, for 2 hours before treating the cells with AA-d8. We treated the pretreated senescent

MCF7 cells with AA-d8 (100 μM) in the presence of Cay-10404 overnight. We then removed the Cay-10404 from the treatment medium and incubated the cells with AA-d8 for 0.25, 0.5, and 1 hour. We then fixed the cells and performed hyperspectral Raman imaging. Spectral heatmaps of the senescent MCF7 in the regions 2220±17.5 cm^{-1} and 2254±17.5 cm^{-1} showed intracellular accumulation of AA-d8 in the senescent cells, predominantly in the perinuclear region (Figure 2C). We also observed a heterogeneous intensity distribution of AA-d8 in the perinuclear region, suggesting a heterogeneity in the intracellular accumulation of Arachidonic Acid. We analyzed the hyperspectral Raman images of senescent cells treated with AA-d8 by ratiometric analysis of spectral heatmaps of spectral shifts corresponding to (C=C)-D stretching to CH_2 stretching (Figure 2D) and observed a time-dependent decrease in the major peak (2254 cm^{-1}) intensity normalized to total lipids (2850 cm^{-1}) after removal of COX2 inhibitor (Figure 2E) similar to that in the *in vitro* metabolism of AA-d8 (Figure 2B), suggesting metabolism of arachidonic acid in senescent MCF7 cells. We also observed a decrease in the peak intensity of the minor peak (2220 cm^{-1}) normalized to total lipids (2850 cm^{-1}) at 1 hour after removal of the COX2 inhibitor. These observations suggest the detection of the metabolism of arachidonic acid in senescent MCF7 cells after removal of the COX2 inhibitor by Raman microscopy. This approach demonstrates that Raman spectroscopy of deuterated arachidonic acid can monitor COX2-driven metabolism both in vitro and in cells. Beyond validating COX2 inhibition, this strategy opens the possibility of screening inhibitors of other enzymes in arachidonic acid pathways. By coupling enzymatic assays with hyperspectral Raman imaging, one can spatially and temporally map lipid metabolism in senescent cells at high resolution. This capacity to resolve metabolic heterogeneity without labels establishes Raman microscopy as a powerful chemical biology

tool—enabling precise dissection of senescence-associated lipid pathways and accelerating discovery of selective interventions against senescent cell function.

FIGURES

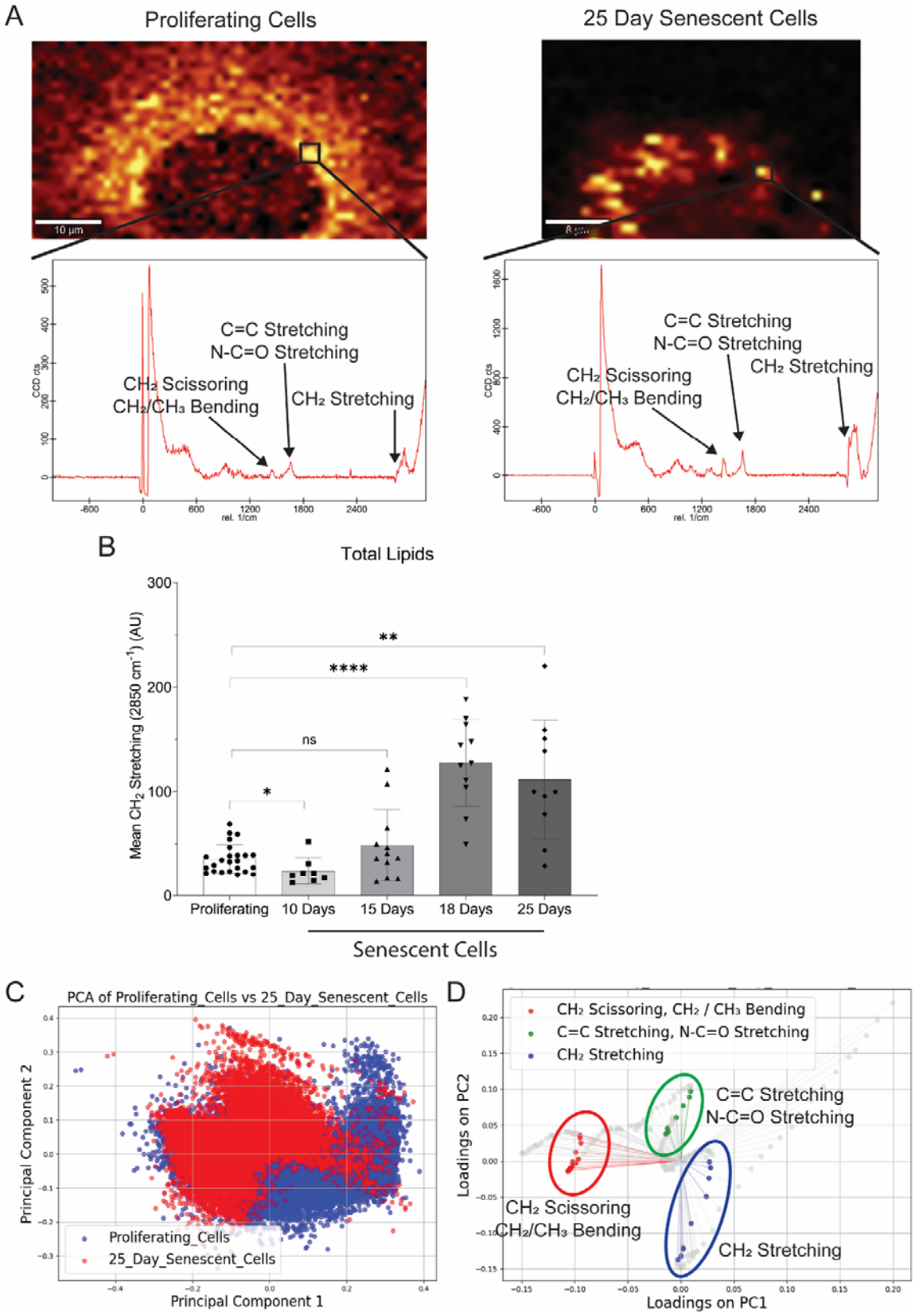
A
Proliferating Cells
25 Day Senescent Cells
10 µm
C=C Stretching
N-C=O Stretching
CH₂ Scissoring
CH₂/CH₃ Bending
CH₂ Stretching
CCD cts
rel. 1/cm
B
Total Lipids
Mean CH₂ Stretching (2850 cm⁻¹) (AU)
ns
*
****
**
Proliferating
10 Days
15 Days
18 Days
25 Days
Senescent Cells
C
PCA of Proliferating_Cells vs 25_Day_Senescent_Cells
Principal Component 2
Principal Component 1
Proliferating_Cells
25_Day_Senescent_Cells
D
CH₂ Scissoring, CH₂ / CH₃ Bending
C=C Stretching, N-C=O Stretching
CH₂ Stretching
Loadings on PC2
Loadings on PC1

Figure 1: Visualization of intracellular biomolecular composition of senescent cells using Hyperspectral Raman Imaging.

A. Spectral heatmaps of the 2850 cm^{-1} (CH_2 Stretching) region and representative Raman spectrum in the proliferating and 25-day senescent MCF7 human breast adenocarcinoma cells.

B. Averaged intensity 2850 cm^{-1} (CH_2 Stretching) peak obtained from hyperspectral Raman Imaging of MCF7 human breast adenocarcinoma cells during proliferation and DNA-damage mediated senescence.

C. Principal Component Analysis of Hyperspectral Raman images of MCF7 human breast adenocarcinoma cells during proliferation and 25 days after induction of DNA damage-mediated senescence.

D. Scatter plot of the projected loadings of Raman shifts' contribution to the principal components PC1 and PC2. Red highlighted points show projected loadings of Raman shifts corresponding to CH_2 scissoring or CH_2/CH_3 Bending (1445 cm^{-1}), green points show projected loadings of Raman shifts corresponding to C=C Stretching or N-C=O Stretching (1655 cm^{-1}), and blue points show projected loadings of Raman shifts corresponding to CH_2 Stretching (2850 cm^{-1})

(The Standard Deviation between replicates was plotted as error bars. Statistical significance was tested by the two-tailed Student's *t*-test ns = $p > 0.05$, *$p < 0.05$, **$p < 0.01$, ***$p < 0.001$, ****$p < 0.0001$.)

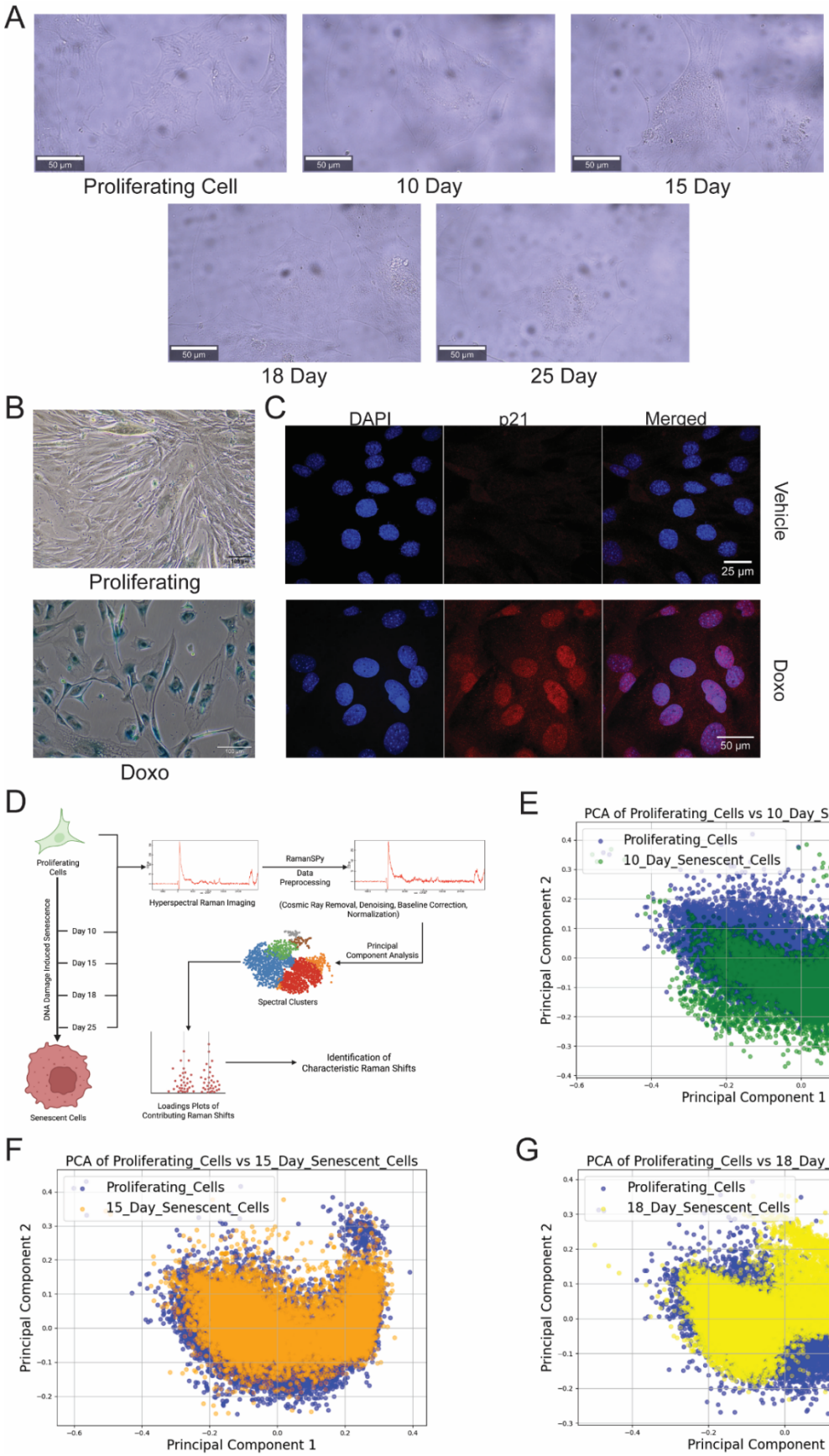
A
Proliferating Cell
10 Day
15 Day
18 Day
25 Day
B
Proliferating
Doxo
C
DAPI
p21
Merged
Vehicle
Doxo
25 µm
50 µm
D
Proliferating Cells
Senescent Cells
DNA Damage Induced Senescence
Day 10
Day 15
Day 18
Day 25
Hyperspectral Raman Imaging
RamanSPy
Data Preprocessing
(Cosmic Ray Removal, Denoising, Baseline Correction, Normalization)
Principal Component Analysis
Spectral Clusters
Loadings Plots of Contributing Raman Shifts
Identification of Characteristic Raman Shifts
E
PCA of Proliferating_Cells vs 10_Day_Senescent_Cells
Proliferating_Cells
10_Day_Senescent_Cells
Principal Component 1
Principal Component 2
F
PCA of Proliferating_Cells vs 15_Day_Senescent_Cells
Proliferating_Cells
15_Day_Senescent_Cells
Principal Component 1
Principal Component 2
G
PCA of Proliferating_Cells vs 18_Day_Senescent_Cells
Proliferating_Cells
18_Day_Senescent_Cells
Principal Component 1
Principal Component 2

Supplementary Figure S1: Visualization of intracellular biomolecular composition of senescent cells using Hyperspectral Raman Imaging.

A. Morphology of MCF7 human breast adenocarcinoma cells during DNA damage-mediated senescence.

B. Expression of senescence-associated β-galactosidase enzyme (SA β-gal) in MCF7 human breast adenocarcinoma cells after DNA damage-mediated senescence.

C. Expression and nuclear accumulation of tumor suppressor p21 in MCF7 human breast adenocarcinoma cells after DNA damage-mediated senescence.

D. Schematic Representation of the workflow to analyze Hyperspectral Raman images of MCF7 cells at different timepoints after Doxo-mediated DNA damage.

E. Visualization of proliferating and 10-day senescent MCF7 cells on the PC plot.

F. Visualization of proliferating and 15-day senescent MCF7 cells on the PC plot.

G. Visualization of proliferating and 18-day senescent MCF7 cells on the PC plot.

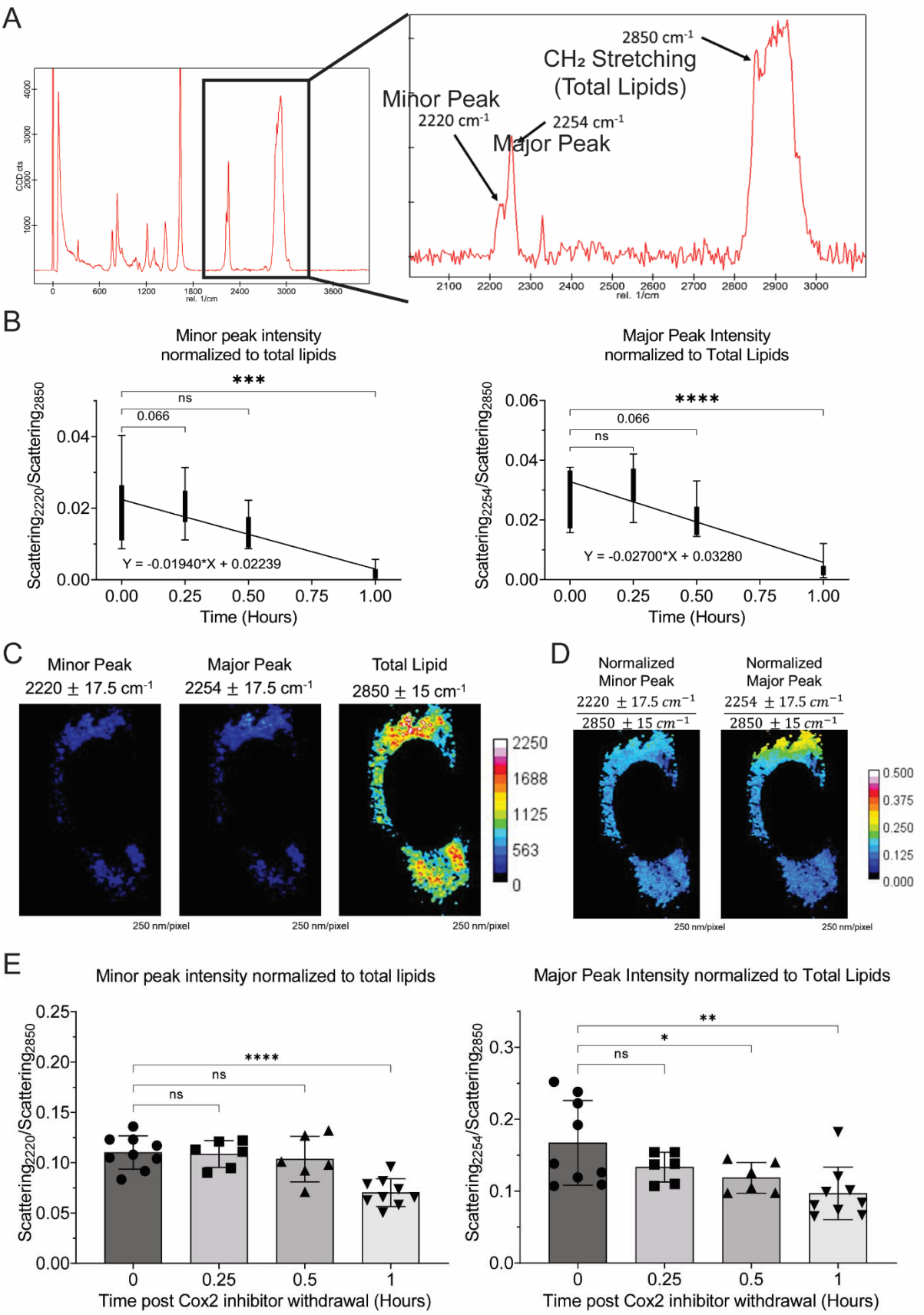
A
2850 cm-1
CH₂ Stretching
(Total Lipids)
Minor Peak
2220 cm-1
2254 cm-1
Major Peak
CCD cts
rel. 1/cm
B
Minor peak intensity
normalized to total lipids
Scattering2220/Scattering2850
***
ns
0.066
Y = -0.01940*X + 0.02239
Time (Hours)
Major Peak Intensity
normalized to Total Lipids
Scattering2254/Scattering2850
****
0.066
ns
Y = -0.02700*X + 0.03280
Time (Hours)
C
Minor Peak
2220 ± 17.5 cm-1
Major Peak
2254 ± 17.5 cm-1
Total Lipid
2850 ± 15 cm-1
2250
1688
1125
563
0
250 nm/pixel
D
Normalized
Minor Peak
2220 ± 17.5 cm−1 / 2850 ± 15 cm−1
Normalized
Major Peak
2254 ± 17.5 cm−1 / 2850 ± 15 cm−1
0.500
0.375
0.250
0.125
0.000
250 nm/pixel
E
Minor peak intensity normalized to total lipids
Scattering2220/Scattering2850
****
ns
ns
Time post Cox2 inhibitor withdrawal (Hours)
Major Peak Intensity normalized to Total Lipids
Scattering2254/Scattering2850
**
*
ns
Time post Cox2 inhibitor withdrawal (Hours)

Figure 2. Visualization of Arachidonic Acid Metabolism in senescent MCF7 cells using hyperspectral Raman imaging of deuterated arachidonic acid.

A. Raman spectrum of 5,6,8,9,11,12,14,15 D8 – Arachidonic Acid (AA-d8) showing two modes of signature spectral shifts of (C=C)-D stretching in the biologically silent region at 2220 cm^{-1} (minor peak) and 2254 cm^{-1} (major peak).

B. Intensity of the two (C=C)-D stretching peaks (2220 and 2254 cm^{-1}) normalized to the intensity of the total lipids peak (CH_2 Stretching, 2850 cm^{-1}) measured by Raman spectroscopy at different timepoints during -mediated metabolism of Arachidonic Acid in *vitro.*

C. Visualization of the intracellular distribution of AA-d8 in senescent MCF7 cells by hyperspectral Raman imaging.

D. Ratiometric heatmaps for visualization of the intracellular distribution of AA-d8 in senescent MCF7 cells by hyperspectral Raman imaging.

E. Intensity of the two (C=C)-D stretching peaks (2220 and 2254 cm^{-1}) normalized to the intensity of the total lipids peak (CH_2 Stretching, 2850 cm^{-1}) measured by hyperspectral Raman imaging in senescent MCF7 cells at different timepoints after removal of COX2 inhibitor (CAY 10404).

(The Standard Deviation between replicates was plotted as error bars. Statistical significance was tested by the two-tailed Student's *t*-test ns = $p > 0.05$, *$p < 0.05$, **$p < 0.01$, ***$p < 0.001$, ****$p < 0.0001$.)

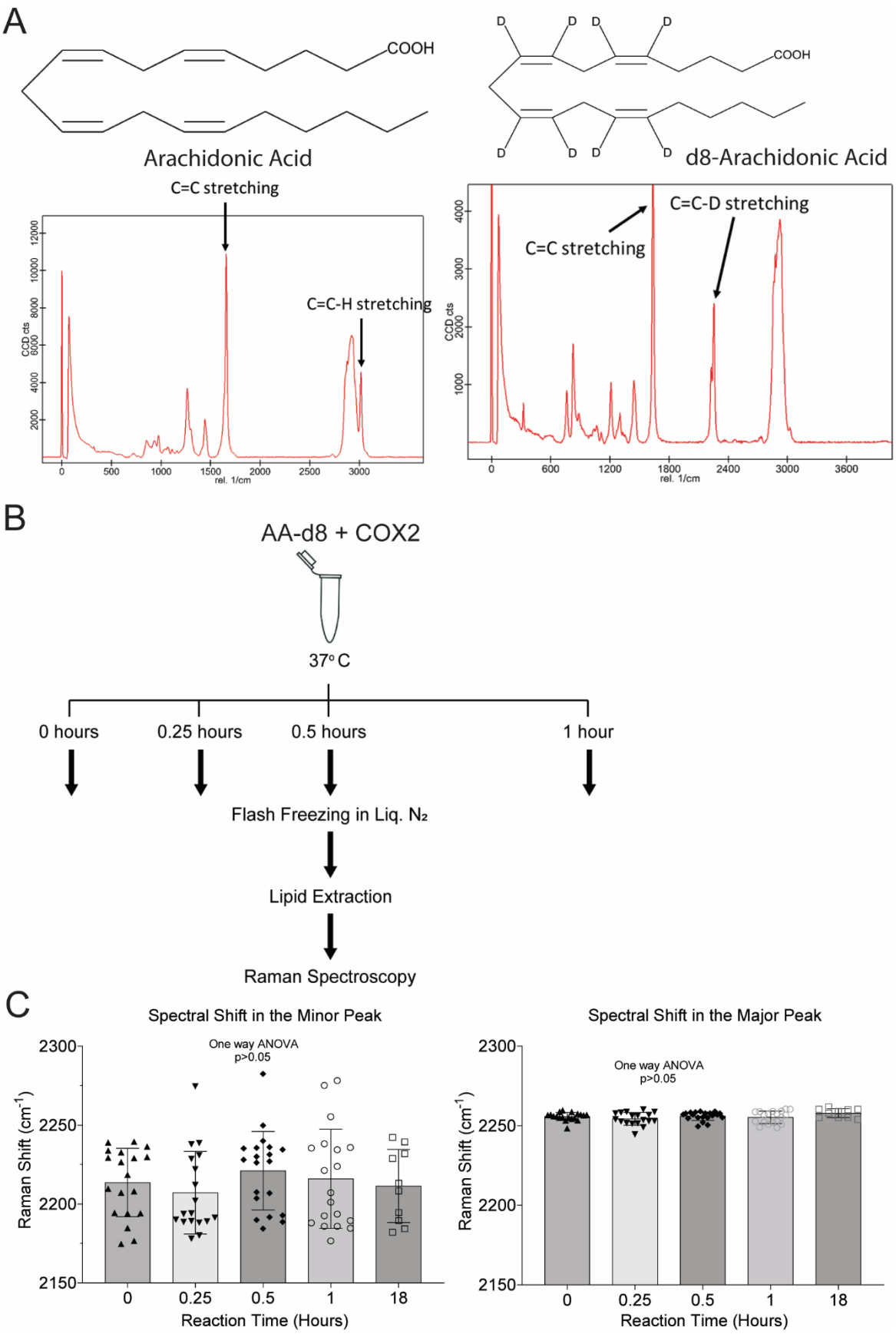
A
COOH
Arachidonic Acid
D
COOH
d8-Arachidonic Acid
C=C stretching
C=C-H stretching
CCD cts
rel. 1/cm
C=C-D stretching
C=C stretching
B
AA-d8 + COX2
37° C
0 hours
0.25 hours
0.5 hours
1 hour
Flash Freezing in Liq. N₂
Lipid Extraction
Raman Spectroscopy
C
Spectral Shift in the Minor Peak
One way ANOVA
p>0.05
Raman Shift (cm⁻¹)
Reaction Time (Hours)
Spectral Shift in the Major Peak
One way ANOVA
p>0.05
Raman Shift (cm⁻¹)
Reaction Time (Hours)

Supplementary Figure S2: Visualization of Arachidonic Acid Metabolism using hyperspectral Raman imaging of deuterated arachidonic acid.

A. Raman spectra of Arachidonic Acid and AA-d8 showing the presence of spectral shifts corresponding to (C=C)-H stretching (3005 cm^{-1}) and (C=C)-D Stretching (2220 and 2254 cm^{-1}), respectively.

B. Schematic Representation of the COX2-mediated metabolism of AA-d8 *in vitro*.

C. Spectral shift wavenumbers corresponding to (C=C)-D Stretching in AA-d8 at different timepoints during COX2-mediated metabolism *in vitro*.

AUTHOR INFORMATION

Corresponding Author

Dr. Arvind Ramanathan

Metabolic Regulation of Cell Fate (RCF), Institute for Stem Cell Science and Regenerative Medicine (BRIC-InStem), GKVK – Post, Bellary Road, Bengaluru – 560065.

Contact: arvind@instem.res.in

Author Contributions

SSP and AR conceptualized the project, designed experimental protocols and analysis pipelines, and wrote the manuscript. SSP did the *in vitro* biochemical experiments, Raman Imaging, and Image processing (both ImageJ and RamanSPy). AV performed the cell culture experiments, helped with Image processing (RamanSPy), and manuscript edits. HM helped with reagent procurement and Raman imaging and analysis. AR funded the project and is the corresponding author. The manuscript was written through contributions of all authors. All authors have given approval to the final version of the manuscript.

Funding Sources

ACKNOWLEDGMENT

The authors thank the Central Imaging and Flow Cytometry Facility (NCBS-InStem) for the imaging solutions. The Authors thank Prof. Satyajit Mayor and Prof. Chandrabhas Narayana for their valuable inputs in the study

ABBREVIATIONS:

DNA: Deoxyribonucleic Acid, SASP: Senescence Associated Secretory Phenotype, MCF7: Human Breast Adenocarcinoma Cell Line Michigan Cell Foundation 7, PCA: Principal Component Analysis, AA-d8: 5,6,8,9,11,12,14,15 D8 – Arachidonic Acid, COX2: Cyclooxygenase 2 enzyme, Doxo: Doxorubicin, PUFA: Polyunsaturated Fatty Acids, DMEM: Dulbecco's Modified Eagle Medium, FBS: Fetal Bovine Serum, DMSO: Dimethyl Sulphoxide, DPBS: Dulbecco's Phosphate Buffer Saline, EDTA: Ethylenediaminetetraacetic Acid

REFERENCES

(1) Di Leonardo, A.; Linke, S. P.; Clarkin, K.; Wahl, G. M. DNA Damage Triggers a Prolonged P53-Dependent G1 Arrest and Long-Term Induction of Cip1 in Normal Human Fibroblasts. *Genes Dev.* **1994**, *8* (21), 2540–2551. https://doi.org/10.1101/gad.8.21.2540.

(2) Robles, S. J.; Adami, G. R. Agents That Cause DNA Double Strand Breaks Lead to P16(INK4a) Enrichment and the Premature Senescence of Normal Fibroblasts. *Oncogene* **1998**, *16* (9), 1113–1123. https://doi.org/10.1038/sj.onc.1201862.

(3) Hu, X.; Zhang, H. Doxorubicin-Induced Cancer Cell Senescence Shows a Time Delay Effect and Is Inhibited by Epithelial-Mesenchymal Transition (EMT). *Med. Sci. Monit.* **2019**, *25*, 3617–3623. https://doi.org/10.12659/MSM.914295.

(4) Campisi, J. Senescent Cells, Tumor Suppression, and Organismal Aging: Good Citizens, Bad Neighbors. *Cell* **2005**, *120* (4), 513–522. https://doi.org/10.1016/j.cell.2005.02.003.

(5) Dilley, T. K.; Bowden, G. T.; Chen, Q. M. Novel Mechanisms of Sublethal Oxidant Toxicity: Induction of Premature Senescence in Human Fibroblasts Confers Tumor Promoter Activity. *Exp. Cell Res.* **2003**, *290* (1), 38–48. https://doi.org/10.1016/S0014-4827(03)00308-2.

(6) Coppé, J. P.; Desprez, P. Y.; Krtolica, A.; Campisi, J. The Senescence-Associated Secretory Phenotype: The Dark Side of Tumor Suppression. *Annu. Rev. Pathol. Mech. Dis.* **2010**, *5*, 99–118. https://doi.org/10.1146/annurev-pathol-121808-102144.

(7) Wiley, C. D.; Campisi, J. The Metabolic Roots of Senescence: Mechanisms and Opportunities for Intervention. *Nat. Metab. 2021 310* **2021**, *3* (10), 1290–1301. https://doi.org/10.1038/s42255-021-00483-8.

(8) Wiley, C. D.; Sharma, R.; Davis, S. S.; Lopez-Dominguez, J. A.; Mitchell, K. P.; Wiley, S.; Alimirah, F.; Kim, D. E.; Payne, T.; Rosko, A.; Aimontche, E.; Deshpande, S. M.; Neri, F.; Kuehnemann, C.; Demaria, M.; Ramanathan, A.; Campisi, J. Oxylipin Biosynthesis Reinforces Cellular Senescence and Allows Detection of Senolysis. *Cell Metab.* **2021**, *33* (6), 1124-1136.e5. https://doi.org/10.1016/j.cmet.2021.03.008.

(9) Kumamoto, Y.; Harada, Y.; Takamatsu, T.; Tanaka, H. Label-Free Molecular Imaging and Analysis by Raman Spectroscopy. *ACTA Histochem. Cytochem.* **2018**, *51* (3), 101–110. https://doi.org/10.1267/AHC.18019.

(10) Pundlik, S. S.; Barik, A.; Venkateshvaran, A.; Sahoo, S. S.; Jaysingh, M. A.; Math, R. G.; Lal, H.; Hashmi, M. A.; Ramanathan, A. Senescent Cells Inhibit Mouse Myoblast Differentiation via the SASP-Lipid 15d-PGJ2 Mediated Modification and Control of HRas. *Elife* **2024**, *13*. https://doi.org/10.7554/ELIFE.95229.

(11) Georgiev, D.; Pedersen, S. V.; Xie, R.; Fernández-Galiana, Á.; Stevens, M. M.; Barahona, M. RamanSPy: An Open-Source Python Package for Integrative Raman Spectroscopy Data Analysis. *Anal. Chem.* **2024**, *96* (21), 8492–8500. https://doi.org/10.1021/ACS.ANALCHEM.4C00383/SUPPL_FILE/AC4C00383_SI_003.PDF.

(12) Kuilman, T.; Michaloglou, C.; Mooi, W. J.; Peeper, D. S. The Essence of Senescence. *Genes Dev.* **2010**, *24* (22), 2463–2479. https://doi.org/10.1101/gad.1971610.

(13) Hamsanathan, S.; Gurkar, A. U. Lipids as Regulators of Cellular Senescence. *Front. Physiol.* **2022**, *13*, 796850. https://doi.org/10.3389/FPHYS.2022.796850/BIBTEX.

(14) Vardaki, M. Z.; Gregoriou, V. G.; Chochos, C. L. Biomedical Applications, Perspectives and Tag Design Concepts in the Cell – Silent Raman Window. *RSC Chem. Biol.* **2024**, *5* (4), 273–292. https://doi.org/10.1039/D3CB00217A.